Bioorganic Chemistry 139 (2023) 106677

Contents lists available at ScienceDirect

Bioorganic Chemistry

journal homepage: www.elsevier.com/locate/bioorg

Exploring the chemical space of functionalized [1,2,4]triazolo[4,3-*a*] quinoxaline-based compounds targeting the bromodomain of BRD9

Erica Gazzillo [a,b,1], Martina Pierri [a,b,1], Ester Colarusso [a], Maria Giovanna Chini [c], Maria Grazia Ferraro [d], Marialuisa Piccolo [d], Carlo Irace [d], Ines Bruno [a], Giuseppe Bifulco [a], Stefania Terracciano [a,*], Gianluigi Lauro [a,*]

[a] *Department of Pharmacy, University of Salerno, Via Giovanni Paolo II 132, Fisciano 84084, Italy*
[b] *PhD Program in Drug Discovery and Development, University of Salerno, Via Giovanni Paolo II 132, Fisciano 84084, Italy*
[c] *Department of Biosciences and Territory, University of Molise, C.da Fonte Lappone, Pesche 86090, Italy*
[d] *BioChem Lab, Department of Pharmacy, School of Medicine and Surgery, University of Naples, Via Domenico Montesano 49, Naples 80131, Italy*

ARTICLE INFO

Keywords:
Cancer
Bromodomains
Epigenetics
Virtual screening
Triazoloquinoxaline derivatives
3D pharmacophore models

ABSTRACT

Here we report a detailed structure–activity relationship (SAR) study related to [1,2,4]triazolo[4,3-*a*]quinoxaline-based compounds targeting the reader module of bromodomain containing-protein 9 (BRD9). 3D structure-based pharmacophore models, previously introduced by us, were here employed to evaluate a second generation of compounds, exploring different substitution patterns on the heterocyclic core. Starting from the promising data obtained from our previously identified [1,2,4]triazolo[4,3-*a*]quinoxaline-based compounds **1**–**4**, the combination of *in silico* studies, chemical synthesis, biophysical and *in vitro* assays led to the identification of a new set of derivatives, selected for thoroughly exploring the chemical space of the bromodomain binding site. In more details, the investigation of different linkers at C-4 position highlighted the amine spacer as mandatory for the binding with the protein counterpart and the crucial role of the alkyl substituents at C-1 for increasing the selectivity toward BRD9. Additionally, the importance of a hydrogen bond donor group, critical to anchor the ZA region and required for the interaction with Ile53 residue, was inferred from the analysis of our collected results. Herein we also propose an optimization and an update of our previously reported "pharm-druglike2" 3D structure-based pharmacophore model, introducing it as "pharm-druglike2.1". Compounds **24-26**, **32**, **34** and **36** were identified as new valuable BRD9 binders featuring IC_{50} values in the low micromolar range. Among them, **24** and **36** displayed an excellent selectivity towards BRD9 and a good antiproliferative effect on a panel of leukemia models, especially toward CCRF-CEM cell line, with no cytotoxicity on healthy cells. Notably, the interaction of **24** and **36** with the bromodomain and PHD finger-containing protein 1 (BRPF1) also emerged, disclosing them as new and unexplored dual inhibitors for these two proteins highly involved in leukemia. These findings highlight the potential for the identification of new attractive dual epidrugs as well as a promising starting point for the development of chemical degraders endowed with anticancer activities.

1. Introduction

Epigenetic mechanisms involved in histones regulations influence the overall state of chromatin and, accordingly, the gene expression. Alterations at this level, such as DNA methylation, histone modifications and regulation by small non-coding RNAs, are strongly recognized as key contributors to cancer development and progression [1]. One of the most important post-translational modifications (PTMs) is related to the regulation of the level of acetylation of lysine residues managed by histone acetyltransferases (HATs) as "writers" and histone deacetylases (HDACs) proteins as "erasers". Such epigenetic marks are specifically recognized by specialized proteins with unique domains, called epigenetic "readers", e.g., bromodomains (BRDs), able to recruit additional chromatin modifiers and remodeling enzymes that act as the effectors of these modifications [2]. BRDs are evolutionarily conserved protein domains (~110 amino acids) that selectively bind ε-*N*-acetyl-lysine

* Corresponding authors.
E-mail addresses: sterracciano@unisa.it (S. Terracciano), glauro@unisa.it (G. Lauro).
[1] These authors contributed equally to this work.

https://doi.org/10.1016/j.bioorg.2023.106677
Received 4 April 2023; Received in revised form 8 June 2023; Accepted 10 June 2023
Available online 12 June 2023

residues on histone tails and other substrates [3]. According to the most recent classification, the human BRDs are grouped into eight families that span all 61 domains [2]. Among these families, the BET family (Bromo- and Extra-Terminal-Domain), including BRD2, BRD3, BRD4, and BRDT proteins [4], is the most studied due to its clear involvement in cellular proliferation related to pathological conditions. However, proteins belonging to the BET family represent only a small percentage of the bromodomains identified so far, and new studies and insights are needed toward other bromodomain containing-proteins as well. In this scenario, non-BET BRDs represent important epigenetic targets of pharmaceutical interest given their pivotal biological functions, although further insights are still required [5]. Among the non-BET proteins, bromodomain containing-protein 9 (BRD9), which is involved in chromatin remodeling as an epigenetic reader able to recognize acetylated lysines (KAc) on histone tails, has emerged as an attractive and promising target in the field of cancer treatment. Notably, as a subunit of the mammalian switch/sucrose non-fermentable (SWI/SNF) complex, a chromatin remodeling machinery, it plays a critical role for the onset and survival of cancer forms since its subunits result mutated in 20% of all human cancers [6]. Although its biological role is not yet completely clarified, BRD9 regulates the expression of oncogenes and anti-apoptotic proteins, leading to abnormal cell proliferation and survival in different tumor types, e.g., endometrial carcinoma, non-small cell lung cancer and prostatic adenocarcinoma, and, more importantly, acute myeloid leukaemia (AML) [7–9]. Indeed, BRD9 knockout, as well as its inhibition by small molecules, results in G1-phase blockage of cell proliferation in AML [3,10].

These findings stimulated an intensive research activity on BRD9, as well as the discovery of new small molecules that represent promising tools for the anticancer therapy and to further investigate the biological role of this specific bromodomain. However, the identification of new molecular platforms that selectively bind BRD9, especially over BRD7, still represents a bottleneck mainly due to the structural similarities, the high conservation of acetyllysine binding residues, and the biological functions of different bromodomains.

Taking advantage of a multidisciplinary approach, we proceeded with our research on this epigenetic target [11–14], starting from 4 hit compounds previously identified by us (**1**–**4**, Fig. 1). In this study, we performed an accurate structure–activity relationship study aimed at carefully exploring the chemical space at C-4 and C-1 position on the [1,2,4]triazolo[4,3-*a*]quinoxaline scaffold to disclose new key structural features of a BRD9 binder [15].

Exploiting fast and efficient synthetic procedures, the selected new derivatives (*vide infra*) were obtained, with the final goal of evaluating the influence in the BRD9 binding induced by chemical variations on the aromatic substituent at C-4 on the starting core. Finally, in light of the potentially improved selectivity given by the hydrophobic group at C-1, the replacement of the 1-ethyl chemical function with longer alkyl chains was also investigated, confirming the possibility of accommodating bulkier substituents due to the peculiar conformation of the acetyllysine binding site of BRD9 bromodomain.

2. Results and discussion

2.1. Exploration of the linker at C-4 through computational and preliminary biophysical analysis

As mentioned above, the 1-ethyl-[1,2,4]triazolo[4,3-*a*]quinoxaline scaffold represented a new interesting chemical core to be further investigated in order to disclose new potent and selective BRD9 binders. In more detail, this motif was identified by us after developing 3D structure-based pharmacophore models [15] (Figure S1), which were once again here implemented for exploring the chemical space to select new putative derivatives. Since the starting 1-ethyl-[1,2,4]triazolo[4,3-*a*]quinoxaline scaffold respected all the pharmacophoric points of the "pharm-fragment" pharmacophore model (Fig. S1A), the initial chemical modifications were selectively related to the substituent at the C-4 position, in order to obtain new derivatives able to respect the features of the "pharm-druglike2" model (Fig. S1C). Moreover, the C-4 position is easily accessible taking into account different synthetic routes, and this would allow a wide exploration of the ZA channel of BRD9 binding site through specific decorations of the heterocyclic scaffold. Specifically, 30 new derivatives (**5**–**34**, Table 1) were selected to evaluate both the influence of various chemical modifications, as well as the length and the nature of different spacer types, i.e., amine linker, direct C—C bond, amide and ether linker. Moreover, based on the key ability of BRD9 to tolerate bulky alkyl groups in the region responsible for the acetyllysine recognition when compared with other bromodomains [16], two additional derivatives (**35**–**36**, Table 1) were synthesized after replacing the ethyl at C-1 of the triazoloquinoxaline scaffold with propyl and butyl substituents. In more detail, the general multidisciplinary workflow shown in Fig. 2 was here applied and reiterated for the selection and evaluation of the compounds, performing a careful SAR study.

Firstly, with the aim of exploring the chemical space of the BRD9 binding pocket and to better clarify how new binders can be accommodated, the amine linker between the central core and the substituent at C-4, originally present in compounds **1**–**4**, was replaced with a direct C—C junction, in order to evaluate the effects of the flexibility and the distance between these two molecular frameworks on the binding with the protein counterpart. In detail, these derivatives could be easily obtained by the fast and efficient Suzuki-Miyaura cross-coupling reaction (see Section 2.5). Therefore, accounting for all the commercially available boronic acids, a virtual library was built and subjected to molecular docking experiments and pharmacophore screening (see the general workflow reported in Fig. 2). Finally, 16 new derivatives (**5**–**20**, Table 1) were selected, of which **5** and **6** were chosen as close derivatives of compounds **1** and **2** (Fig. 1) previously identified as effective BRD9 binders. Compounds **7**–**20** were selected on the basis of docking score, PhaseScreen score and as able to respect at least 6/7 of pharmacophoric features of "pharm-druglike2" (Table 1). All the synthesized derivatives **5**–**20** were tested through AlphaScreen assays, and the obtained outcomes clearly highlighted that the absence of a linker between the scaffold and the substituents was detrimental to BRD9 binding (Table 1). Such evidence is due to the absence of a spacing group from the central heterocyclic core and the substituents at C-4, which results in the lack of the necessary length and adequate spatial arrangement of the chemical groups (e.g., acceptor groups) in the binding site of BRD9 (Fig. 3A). In addition, despite the presence of an aromatic scaffold with an acetyllysine mimetic function that enables the establishment of key

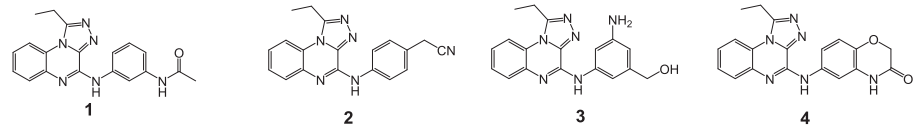

Fig. 1. 2D structures of our previously identified hit compounds **1**–**4**, featuring the 1-ethyl-[1,2,4]triazolo[4,3-*a*]quinoxaline scaffold [15].

Table 1
Chemical structures, *in silico* parameters and detected binding towards BRD9 of compounds **5**–**36** expressed as percentage of residual binding of residual binding of acetyled-Histone H4 (H4Ac) to BRD9 ± SD. Also, IC_{50} ± SD values are reported for compounds **24**-**26**, **32**, **34**, **36**, and Bromosporine.

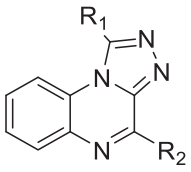

Compound	R_1	R_2	Docking score (kcal/mol)	PhaseScreen score	Num sites matched	Residual binding of H4Ac to BRD9 ± SD (%) [Compound] = 10 μM	IC_{50} ± SD (μM)
5	CH_2CH_3	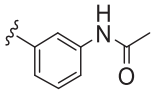	−6.56	1.63	7/7	98.42 ± 6.00	/
6	CH_2CH_3	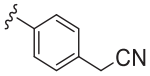	−5.42	1.56	7/7	92.24 ± 5.71	/
7	CH_2CH_3	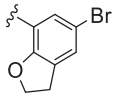	−4.34	1.40	6/7	90.93 ± 1.04	/
8	CH_2CH_3	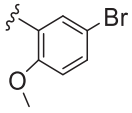	−5.29	1.27	6/7	88.44 ± 2.17	/
9	CH_2CH_3	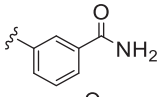	−6.98	1.53	6/7	91.71 ± 0.77	/
10	CH_2CH_3	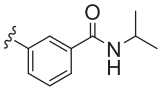	−6.46	1.50	6/7	>100	/
11	CH_2CH_3	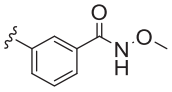	−7.00	1.44	7/7	> 100	/
12	CH_2CH_3	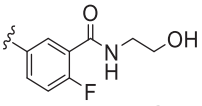	−7.28	1.40	7/7	93.02 ± 0.70	/
13	CH_2CH_3	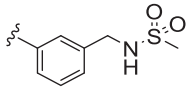	−6.42	1.54	7/7	> 100	/
14	CH_2CH_3	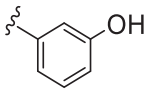	−6.53	1.59	6/7	> 100	/
15	CH_2CH_3	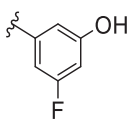	−6.57	1.63	6/7	> 100	/
16	CH_2CH_3	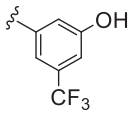	−6.39	1.59	6/7	93.70 ± 1.74	/
17	CH_2CH_3	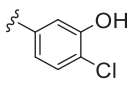	−6.38	1.63	6/7	>100	/
18	CH_2CH_3	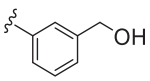	−6.99	1.57	6/7	95.57 ± 2.44	/
19	CH_2CH_3	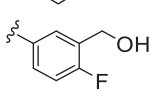	−7.03	1.58	6/7	> 100	/

(*continued on next page*)

Table 1 (*continued*)

Compound	R_1	R_2	Docking score (kcal/mol)	PhaseScreen score	Num sites matched	Residual binding of H4Ac to BRD9 ± SD (%) [Compound] = 10 μM	IC_{50} ± SD (μM)
20	CH_2CH_3	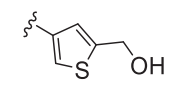	−6.43	1.61	6/7	99.13 ± 0.36	/
21	CH_2CH_3	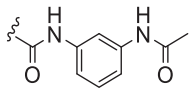	−5.30	1.55	7/7	> 100	/
22	CH_2CH_3	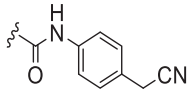	−5.07	1.38	7/7	94.72 ± 3.85	/
23	CH_2CH_3	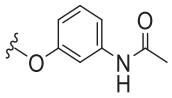	−5.68	1.44	6/7	85.07 ± 2.86	/
24	CH_2CH_3	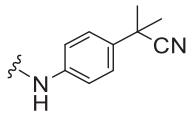	−5.96	1.25	7/7	30.47 ± 1.38	3.93 ± 0.54
25	CH_2CH_3	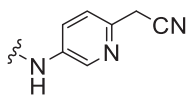	−6.02	1.38	7/7	46.39 ± 0.44	8.24 ± 1.44
26	CH_2CH_3	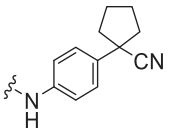	−5.29	1.52	7/7	40.24 ± 0.52	4.41 ± 1.16
27	CH_2CH_3	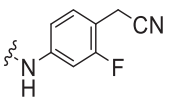	−5.93	1.32	7/7	96.20 ± 2.37	/
28	CH_2CH_3	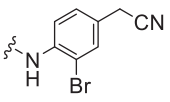	−4.72	1.47	6/7	85.74 ± 9.22	/
29	CH_2CH_3	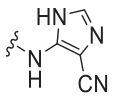	−6.26	1.51	6/7	84.57 ± 4.49	/
30	CH_2CH_3	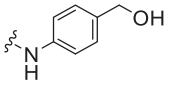	−5.38	1.46	6/7	53.82 ± 7.25	/
31	CH_2CH_3	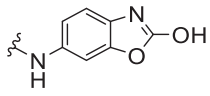	−5.40	1.46	6/7	69.69 ± 1.75	/
32	CH_2CH_3	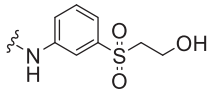	−6.40	1.42	7/7	45.14 ± 0.13	8.31 ± 0.85
33	CH_2CH_3	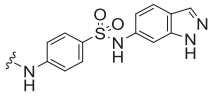	−6.89	1.42	7/7	60.15 ± 0.14	/
34	CH_2CH_3	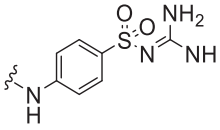	−6.70	1.52	7/7	41.20 ± 4.83	5.26 ± 1.15
35	$CH_2CH_2CH_3$	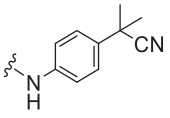	−5.36	1.22	7/7	68.65 ± 1.01	/

(*continued on next page*)

Table 1 (*continued*)

Compound	R_1	R_2	Docking score (kcal/mol)	PhaseScreen score	Num sites matched	Residual binding of H4Ac to BRD9 ± SD (%) [Compound] = 10 μM	IC_{50} ± SD (μM)
36	$CH_2CH_2CH_2CH_3$	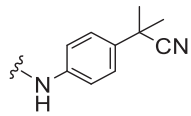	−4.97	1.34	7/7	41.28 ± 2.17	6.73 ± 1.55
Bromosporine	/	/	/	/	/	14.63 ± 1.00	0.42 ± 0.07

interactions with Asn100 and Phe44 for the recognition of BRD9, the absence of a hydrogen bond acceptor/donor group included in the spacing group caused the loss of additional interaction with either Ile53 or Asn100, respectively, depending on the orientation of such group, as shown for compound **5** (Fig. 3A). Moreover, data arising from the pharmacophore screening were partially in line with these results since most of compounds **7**–**20** only matched 6/7 features. Specifically, the H-bond acceptor group, responsible for the interaction with Arg101, represents the missing pharmacophore feature in these compounds that prevents the correct binding with BRD9 due to the absence of a functionalized spacer (see docking pose related to compound **20** in Fig. 3B).

On the basis of the above reported results, the choice of an appropriate linker between the scaffold and the substituents was highlighted as mandatory for obtaining binding towards BRD9. Since all the derivatives did not show promising results, including compounds sharing the same pattern of substitution of bioactive molecules from the first generation, compounds **21**–**23** (Table 1), related to **1** and **2** (Fig. 1), were selected in the subsequent step to further investigate the influence of the linker, specifically accounting for amide and ether linkers. The rationale of the design of derivatives featuring an amide linker (**21**–**22**, Table 1) was related to the evaluation of both the effects of a spacer longer than –NH and direct C—C junction and for the respect of the planar feature "X" of the "pharm-druglike2" model. Moreover, in order to assess the influence of a H-bond acceptor group as linker between the central core and the substituent (i.e., ether linker), compound **23** was also considered for further evaluation. The latter represents a strictly related derivative of **1**, differing from it for the presence of an oxygen functionality instead of a –NH group. Like the first set of derivatives, compounds **21**–**23** were subjected to the same computational protocol (molecular docking experiments and pharmacophore screening) before the synthetic step, in order to assess whether they could *a priori* fulfill the conditions for BRD9 binding. According to the computational results, compounds **21** and **22** respected all the pharmacophoric points (Table 1 and Fig. 3C–D), while compound **23** matched only 6/7 features (Table 1

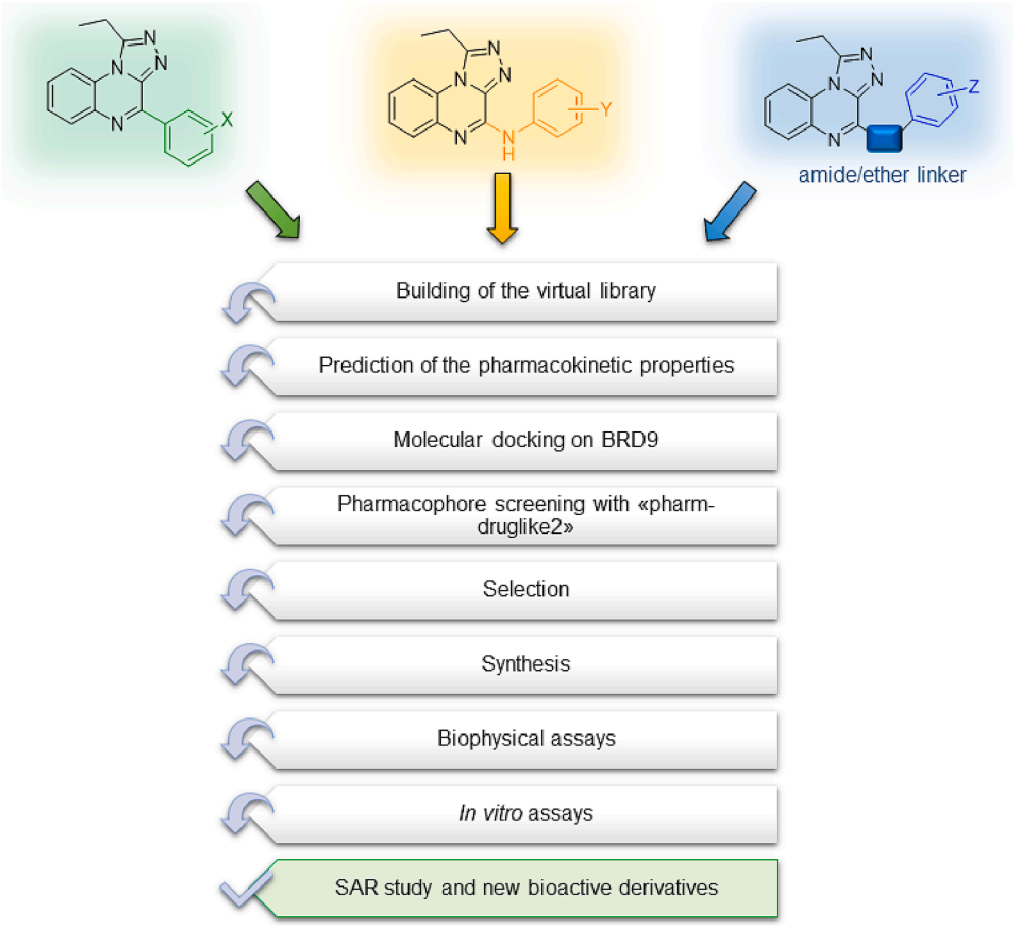

Fig. 2. General workflow applied for the selection of new BRD9 binders.

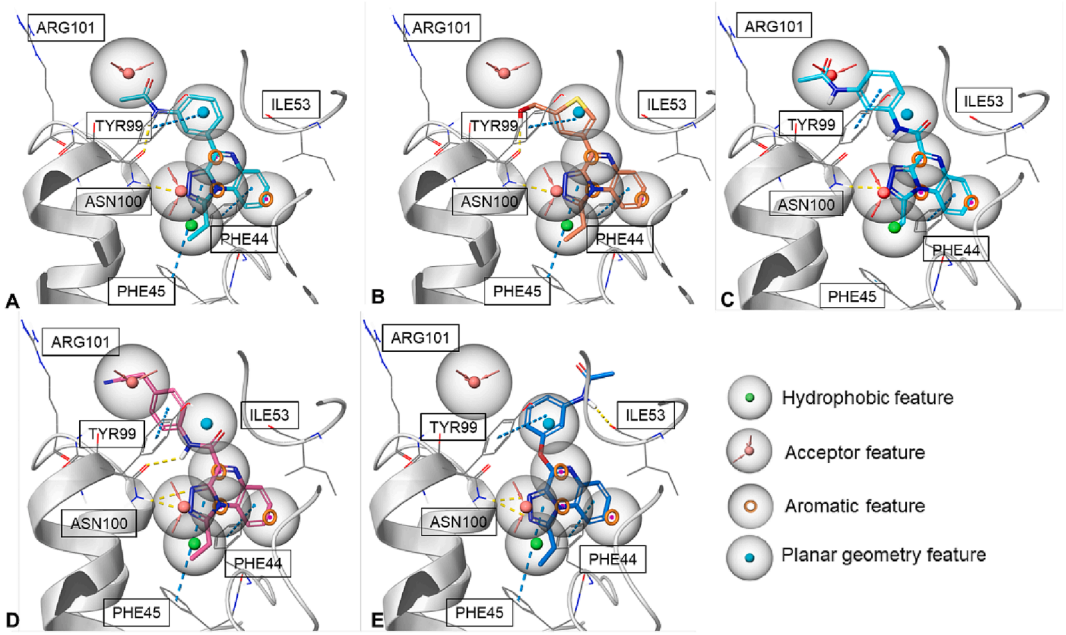

Fig. 3. Binding poses of **5** (panel A), **20** (panel B), **21** (panel C), **22** (panel D), **23** (panel E) in the binding site of BRD9 (PDB code: 5F1H) superimposed on "pharm-druglike2" model. H-bonds and π-π interactions are reported in yellow and cyan dotted lines, respectively. (For interpretation of the references to colour in this figure legend, the reader is referred to the web version of this article.)

and Fig. 3E), due to the loss of the interaction with Arg101. AlphaScreen assays highlighted the absence of activity also for these compounds featuring new different linkers (Table 1), suggesting that an oxygen or carbonyl linked at C-4 position as H-bond acceptor group were detrimental for BRD9 binding, specifically due to the absence and/or poor interaction with the key residue Ile53.

Eventually, since all the above reported modifications at the C-4 linker did not lead to favorable results, we speculated that a donor group at C-4 is required, as demonstrated by the effective BRD9 binding displayed by compounds **1**–**4** [15] and I-BRD9 [17], the latter representing one of the first selective chemical probe identified for BRD9. Accordingly, we re-evaluated the possibility of selecting additional compounds featuring the starting amine linker. In this scenario, a further selection of compounds was made from the previously built virtual library considering the binding data obtained for compounds **1**–**4** (Fig. 1), representing our hit compounds. Starting from these premises, new 11 derivatives (**24**–**34**, Table 1) featuring promising *in silico* parameters, were synthesized accounting for aromatic or heteroaromatic commercially available amines. Specifically, compounds **24**–**29** were selected as close derivatives of **2**, featuring a cyano group on the aromatic substituent at C-4. Moreover, compounds **30**–**32** were included in the selection for the presence of an hydroxy group on the aromatic/heteroaromatic ring at C-4 as in compounds **3**, while **33** and **34** for the presence of sulfonamide moiety, as in high-affinity BRD9 binders (e.g., I-BRD9,

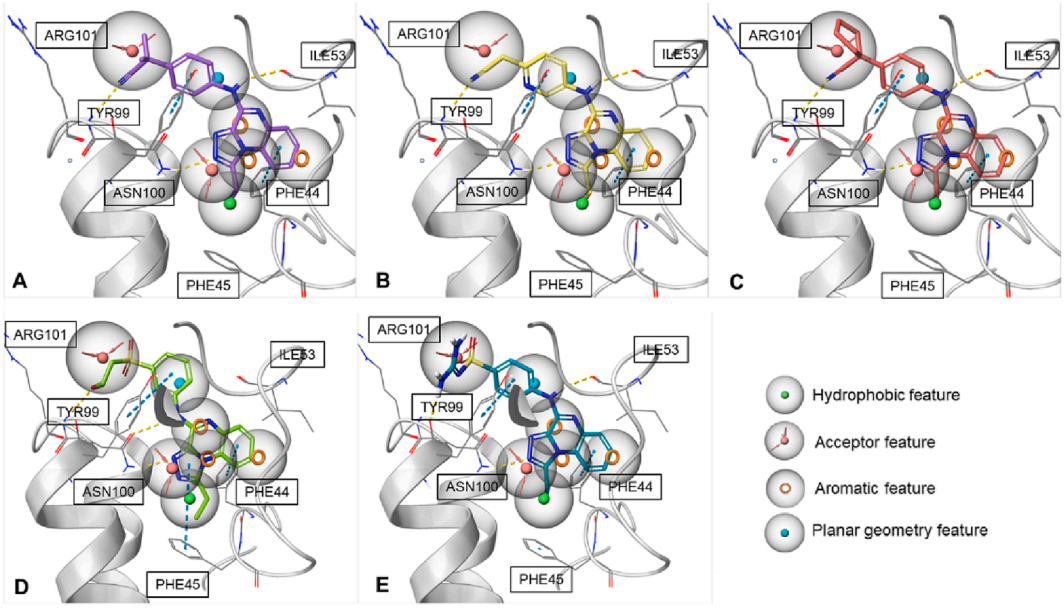

Fig. 4. Binding poses **24** (panel A), **25** (panel B), **26** (panel C), **32** (panel D), and **34** (panel E), in the binding site of BRD9 (PDB code: 5F1H) superimposed on "pharm-druglike2". H-bonds and π-π interactions are reported in yellow and cyan dotted lines, respectively. (For interpretation of the references to colour in this figure legend, the reader is referred to the web version of this article.)

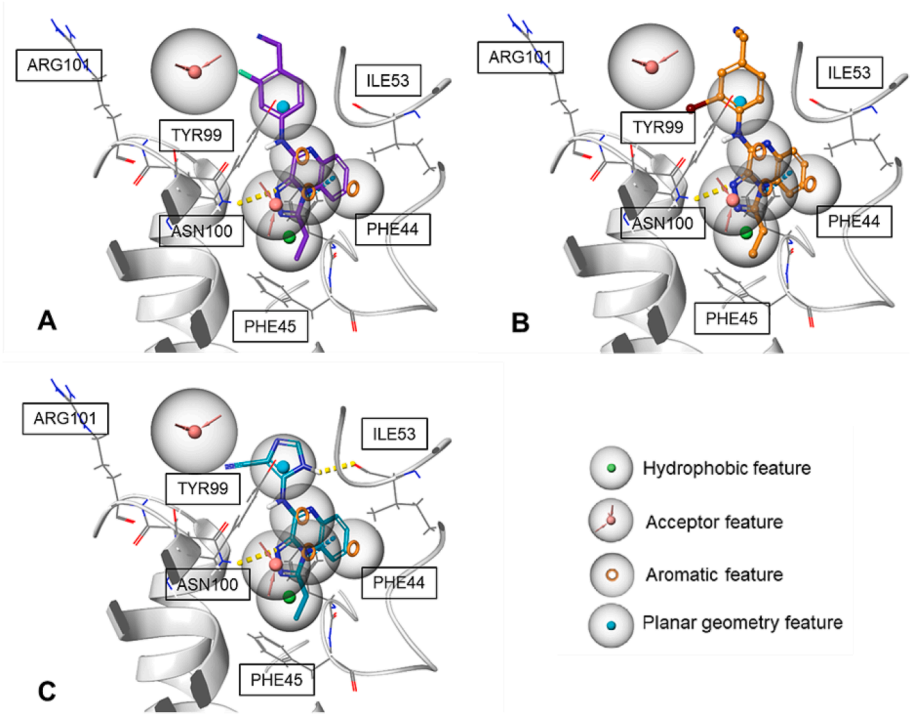

Fig. 5. Binding poses of **27** (panel A), **28** (panel B) and **29** in the binding site of BRD9 (PDB code: 5F1H) superimposed on "pharm-druglike2" model. H-bonds and π-π interactions are reported in yellow and cyan dotted lines, respectively. (For interpretation of the references to colour in this figure legend, the reader is referred to the web version of this article.)

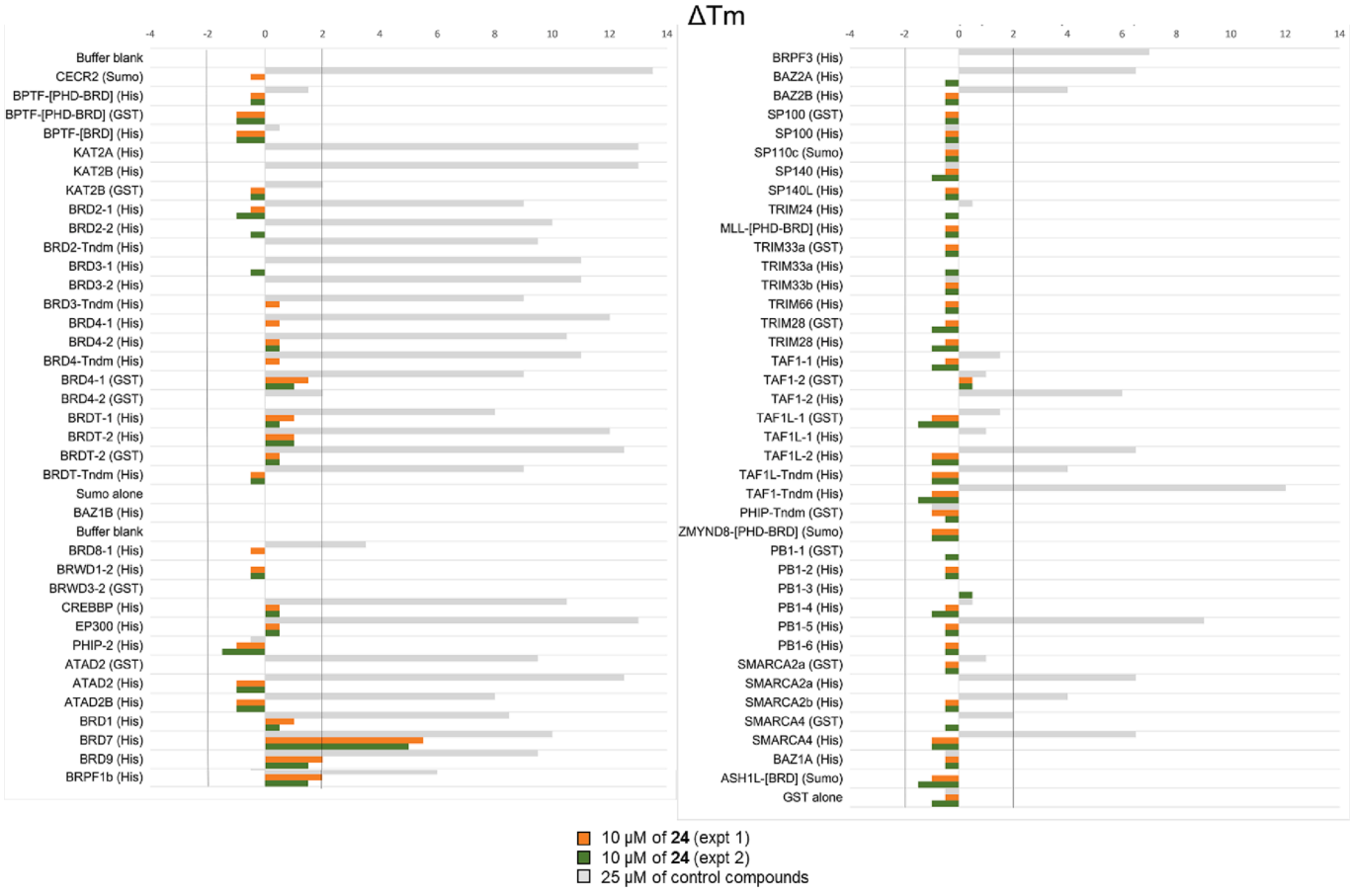

Fig. 6. BromoMELT profile for **24** (10 μM) tested against 76 bromodomains. ΔTm values of control compounds for each bromodomain are also reported.

LP99) [17,18]. The cyano, hydroxy and sulfonamide groups on the aromatic and heteroaromatic ring at C-4 were able to cover the acceptor feature of the "pharm-druglike2". *In silico* data highlighted compounds **24**–**34** as valuable binders and, above all, AlphaScreen assays corroborated such results (Table 1). Indeed, 5 new bioactive compounds were identified (i.e., **24**–**26**, **32**, and **34**) as able to determine H4Ac residual binding < 50% (Table 1 and Fig. 4A-E).

Conversely, compounds **27**–**29** were not able to interfere with the binding between BRD9 and H4Ac (see Table 1). Specifically, the additional presence of a halogen atom in compounds **27** and **28** (Fig. 5A and 5B) as an electron-withdrawing group (i.e., F and Br, respectively) on the aromatic ring led to a decrease in BRD9 binding if compared to the reference compound **2**. On the other hand, **29** did not significantly bind BRD9 since, as reported in Fig. 5C, the cyano group failed to cover the acceptor feature of the "pharm-druglike2" and to establish the key interaction with Arg101. Finally, compound **30** highlighted a moderate interference with the target (Table 1) when compared with the more promising compounds. Considering all the obtained results, we speculated that small modifications of the linker moiety between the central scaffold and the aromatic substituent significantly affect the binding, and in more detail the linker demonstrated to have a dual utility:

1. provide the right length for the necessary interactions to be established between a) Asn100 and Phe44 *vs.* acetyllysine mimetic group; b) Arg101 *vs.* H-bond acceptor group on aromatic substituents;
2. feature an H-bond donor group to establish interaction with Ile53 (Fig. 4A-4C and 4E) or additional interaction with the carbonyl of Asn100 (Fig. 4D).

From the computational models, compounds not complying the aforementioned binding mode (Fig. 4) did not show the ability to bind satisfactorily BRD9 (Fig. 3 and Fig. 5).

2.2. Binding assessment against BRD9 and evaluation of the selectivity profile

For the most interesting compounds belonging to the new synthesized 32 derivatives, i.e., **24**–**26**, **32**, and **34**, IC_{50} determination through AlphaScreen assays was performed, highlighting their binding to BRD9 in the low micromolar range (Table 1 and Figures S2-S5). Moreover, the most promising compound **24** was subjected to an extensive selectivity profile analysis through BromoMELT [19,20] technology, testing it against a panel of 76 bromodomains (Fig. 6).

Interestingly, the BromoMELT confirmed the binding between **24** and BRD9, featuring a $\Delta TM > 2$ °C. Above all, it highlighted the high selectivity of this compound against a large number of members of the human bromodomain family. As expected, a significant binding was also detected for BRD7, probably due to the high sequence identity between BRD9 and BRD7 bromodomains (~72%) [21]. In addition, the binding between **24** and the two isoforms of BRPF1 (BRPF1a and BRPF1b) was also observed. BRPF1 is a subunit of monocytic leukemic zinc finger (MOZ) complex, involved in chromosomal translocations associated with an aggressive subtype of acute myeloid leukemia (AML). BRPF1 enhances the acetylation activity of MOZ, thus representing an interesting target to be modulated [22]. In more detail, different BRPF1 inhibitors were reported [23] and, one crystal structure was deposited on the Protein Data Bank co-complexed with a fragment-like compound featuring the [1,2,4]triazolo[4,3-*a*]quinoxaline scaffold (PDB code: 5EWW), for which binding data and further information were not reported in literature in our knowledge. Moreover, the co-crystallized compound differs from our derivatives by a methyl at C-1 and an alkyl chain at C-4 which, interestingly, represent the positions on the central core subject of our investigations. In light of these, our results represented an interesting outcome worthy of further in-depth studies, considering the dual BRD9/BRPF1 detected binding while also considering the involvement of both targets in leukemia [10,24]. Noteworthy, the most important aspect from BromoMELT investigation was related to the absence of interference with almost all the proteins belonging to the panel of bromodomains accounted, thus corroborating the high selectivity of our [1,2,4]triazolo[4,3-*a*]quinoxaline-based derivatives. In more details, these compounds only significantly bind BRD9 and other two bromodomains, i.e., BRD7 and BRPF1, all belonging to the subfamily 4, while not interfering with bromodomains belonging to the other subfamilies. Starting from these promising results, an accurate investigation on the effect of alkyl substituents at C-1 of the heteroaromatic scaffold was performed in order to enhance the selectivity on BRD9, exploiting the ability of this epigenetic module in accommodating alkyl substituents bulkier than a methyl group [16,25].

2.3. Exploration of the substituent at C-1 through computational and biophysical analysis

After a careful analysis of the chemical modification at C-4 position, compound **24** emerged as a new promising item and was then selected for further investigations and, specifically, our attention was moved to the key C-1 position. As reported above, differently from other bromodomains, BRD9 is able to accommodate bulkier alkyl groups [16]. Such peculiar feature was reported as particularly exploitable for driving the design of new BRD9 probes endowed with high selectivity. On these bases, with the aim to trace a complete structure–activity relationship study, two new derivatives strictly related to compound **24** were synthesized (**35** and **36**, Table 1), accounting for propyl and butyl chemical functions at C-1 position. As expected by our computational prediction, **35** and **36**, which respect all the features of the "pharm-druglike2" (Fig. 7A and 7B), showed an interesting BRD9 binding as confirmed by AlphaScreen assays (Fig. 8 and Table 1). Afterwards, we further validated the ability of compounds **24** and **36** to bind BRD7 and BRPF1, which emerged as promising protein partners from the BromoMELT related to compound **24** (Fig. 6). AlphaScreen experiments confirmed the preliminary BromoMELT outcomes, since **24** and **36** were able to bind BRPF1 in the low micromolar range ($IC_{50} = 4.50 \pm 0.31$ μM and 1.48 ± 0.24 μM, respectively) (Fig. 8 and Table 2). Interestingly, they had a lower affinity toward BRD7, especially with regard to **36** ($IC_{50} = 18.38 \pm 2.06$ μM and 95.76 ± 2.74 μM for **24** and **36**, respectively) (Table 2 and Fig. 8). These results underlined the high selectivity of these compounds and the importance of the introduction of a butyl at C-1, which clearly led to greater selectivity towards BRD9 over BRD7. This evidence is impressive given the high homology of the two proteins and the opposite physiological role that they possess, since BRD7 acts as a tumor suppressor in contrast to BRD9 [26]. Therefore, our findings related to C-1 structural feature provided a compelling achievement to drive the selectivity on BRD9 over BRD7, which represents an important goal in the epigenetic drug discovery. Furthermore, modifications at the C-1 position preserved the binding on BRPF1, highlighting an interesting dual activity on two proteins involved in carcinogenesis and paving the way to a new class of BRD9/BRPF1 epidrugs.

2.4. Preclinical screenings and SAR determination

The bioactivity *in vitro* of the lead compound **24** and its derivative **36** was finally validated by exploiting cellular models of human leukemia. A panel of five leukemia cell lines (i.e., THP-1, Kasumi-1, HL-60, K-562, and CCRF-CEM cells) endowed with different phenotypic features and representing well-established preclinical models of human leukemias (for a detailed description see the Experimental section), were *ad hoc* selected for preliminary bioscreens. As showcased in Figure S6, concentration-effect curves highlight moderate and concentration-dependent antiproliferative effects in all the leukemic models. In an overall vision, almost all the calculated IC_{50} values for compounds **24** and **36** in the indicated leukemia cells are below 100 μM (Table 3), suggestive of a prospective anticancer activity that deserves further investigation. Worthy of note, in the same experimental conditions weak

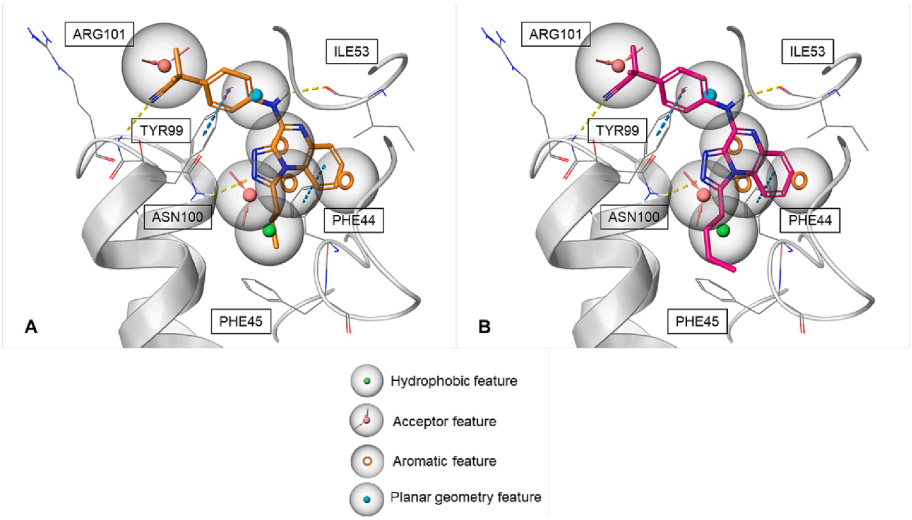

Fig. 7. Binding poses of **35** (panel A) and **36** (panel B), in the binding site of BRD9 (PDB code: 5F1H) superimposed on "pharm-druglike2". H-bonds and π-π interactions are reported in yellow and cyan dotted lines, respectively. (For interpretation of the references to colour in this figure legend, the reader is referred to the web version of this article.)

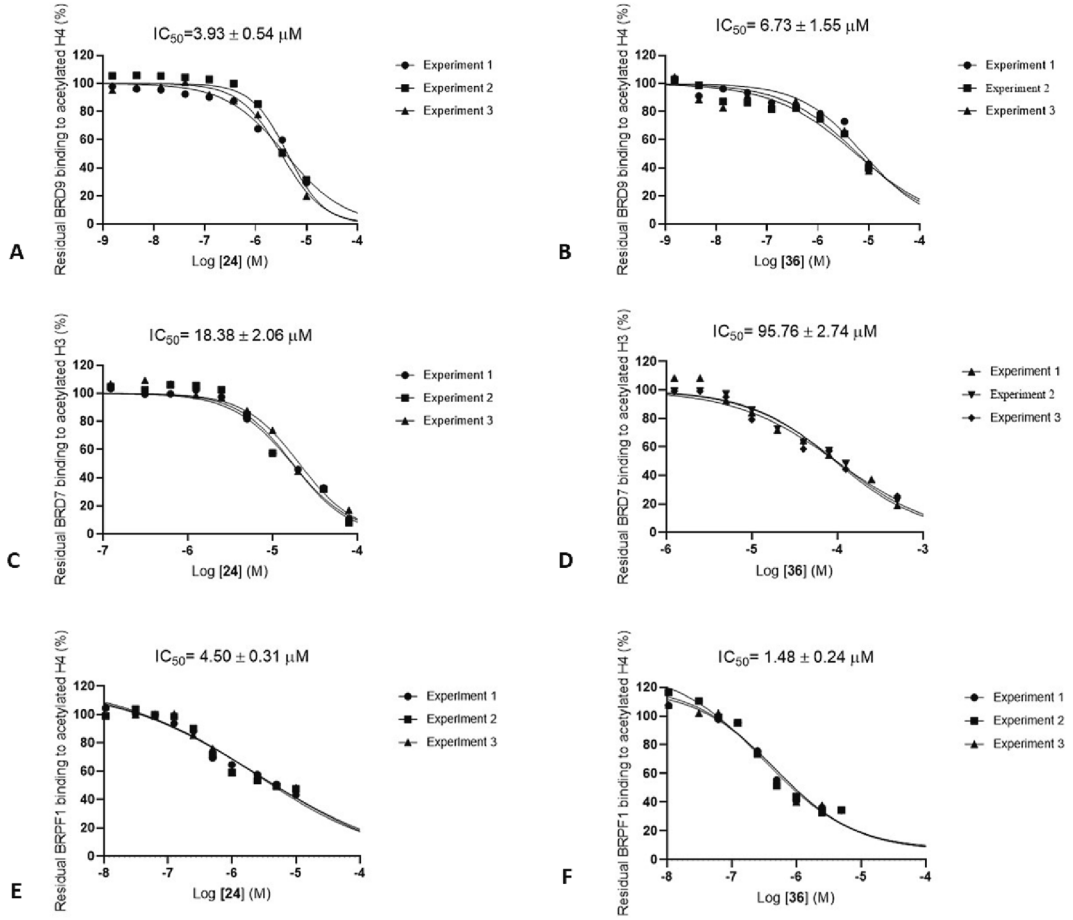

Fig. 8. Concentration-response curves for the analysis of the binding of **24** (left) and **36** (right) on BRD9, BRD7, and BRPF1. Data are expressed as percentage of control (100%), means with SD, n = 3.

or insignificant cytotoxic effects were observed in healthy human cultures (Figure S7), an evidence that can reveal selectivity of action against high replicative cells.

Summarizing, after the evaluation of the new 32 [1,2,4]triazolo[4,3-*a*]quinoxaline-based derivatives (Tables 1 and 2 and Fig. 8), a structure–activity relationship (SAR) profile (Fig. 9) for BRD9 binding can be traced as follows:

- the respect of "pharm-fragment" (including the acetyllysine mimetic group) represents the minimum structural requirement;

Table 2
IC_{50} ± SD values for the newly identified derivatives **24** and **36**, and I-BRD9 and bromosporine employed as control compounds against BRD9, BRD7 and BRPF1. Values are shown as average of three separate experiments.

Compound	BRD9 IC_{50} ± SD (μM)	BRD7 IC_{50} ± SD (μM)	BRPF1 IC_{50} ± SD (μM)
24	3.93 ± 0.54	18.38 ± 2.06	4.50 ± 0.31
36	6.73 ± 1.55	95.76 ± 2.74	1.48 ± 0.24
I-BRD9	0.018 ± 2.1	3.22 ± 0.63	n.t.
Bromosporine	0.42 ± 0.07	n.t.	1.60 ± 0.27

n.t.: not tested.

Table 3
IC_{50} values (μM) relative to **24** and **36** in the listed human leukemia cell lines and healthy cells following 48 h of incubation.

Compound	IC_{50} Cell lines (μM)						
	THP-1	Kasumi-1	HL-60	K-562	CCRF-CEM	HaCaT	HDFa
24	95 ± 6	97 ± 4	> 100	90 ± 5	50 ± 5	> 100	> 100
36	60 ± 5	72 ± 5	81 ± 5.5	65 ± 4	35 ± 4	> 100	> 100

- the direct C—C junction, ether linker and amide linker at C-4 are not tolerated;
- halogen atoms on the substituents at C-4 are not tolerated;
- a linker with one spacer and hydrogen bond donor properties between the central scaffold (at C-4) and the substituent oriented towards ZA loop is tolerated;
- the substituents at C-4 position require aromatic or heteroaromatic rings with a number of atoms > 6;
- the aromatic group at C-4 position requires *para*-substitution with a H-bond acceptor feature;
- alkyl groups featuring up to 4 carbon atoms can be tolerated at C-1 position.

Based on these considerations, we here propose an optimization of the "pharm-druglike2" in which a new H-bond donor feature "D" is inserted close to the planar feature "X" (Fig. 10), resulting in the so-called "pharm-druglike2.1", which efficiently rationalizes all the outcomes reported in this work. Specifically, considering the binding pose of I-BRD9, there are two donor groups, i.e., the two nitrogens of the amidine moiety, which establish two hydrogen bonds with Asn100 and Ile53. The new feature "D", indicated with the yellow arrow in Fig. 10A, was added by taking the nitrogen coordinates of the amidine of I-BRD9 as reference, responsible for hydrogen bonding with Ile53 (Fig. 10B). After a careful analysis of the binding poses, we speculated that this additional interaction between the –NH chemical function of the amidine and Ile53, peculiar to I-BRD9, is important for the selectivity and activity demonstrated by this chemical probe. In summary, a similar binding mode was highlighted when comparing the known inhibitor I-BRD9 and the most active compounds **24** and **36**, as shown in the Fig. 10B-10D. In more detail, I-BRD9, **24** and **36** show a common interaction pattern, involving the establishment of key interactions with a) Asn100 e Phe44 with the acetyllysine mimetic group; b) H-bond between Ile53 and the donor chemical group present in the linker of the considered compounds; c) H-bond between Arg101 and the acceptor chemical group on the substituents. Moreover, **24** and **36** established an additional π-π interaction with Tyr99 due to the presence of an aromatic substituent in the region occupied by the cyclic sulfone in I-BRD9. Interestingly, since I-BRD9 showed a further interaction with Asn100 through the nitrogen of the amidine group, we believe that derivatives featuring chemical groups with two hydrogen bond donor moieties (e.g., amidine as in I-BRD9) may be convenient for further improving the binding towards BRD9. Eventually, as expected, the most active compounds **24** and **36** (Fig. 10C and 10D, respectively) fit perfectly in the volume of the new "D" feature, establishing an H-bond with Ile53, as occurred for I-BRD9. In this scenario, **24** and **36** represent two highly promising molecular platforms since they featured a good selectivity profile regarding BRD9 and binding affinities in the low micromolar range. These compounds will be further investigated for the development of new molecular glues and chemical degraders, since the encouraging obtained results prompt us to optimize and functionalize these newly identified ligands [27].

Finally, to corroborate the SAR profile here traced and to quantitatively evaluate our results, we performed a ligand-based investigation using AutoQSAR tool (Schrödinger Suite) (see Supporting Information). Specifically, we analyzed two different models: a) a first one by considering the "training set 1" (Figure S8); b) a second one by

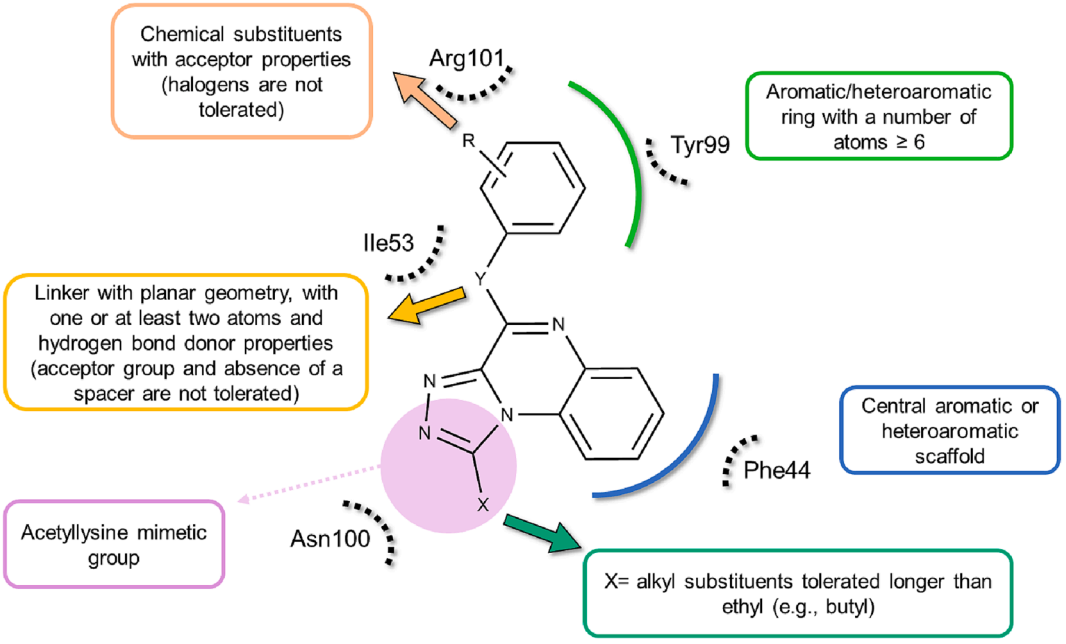

Fig. 9. Representation of the SAR study and the related key points for the design of new BRD9 binders.

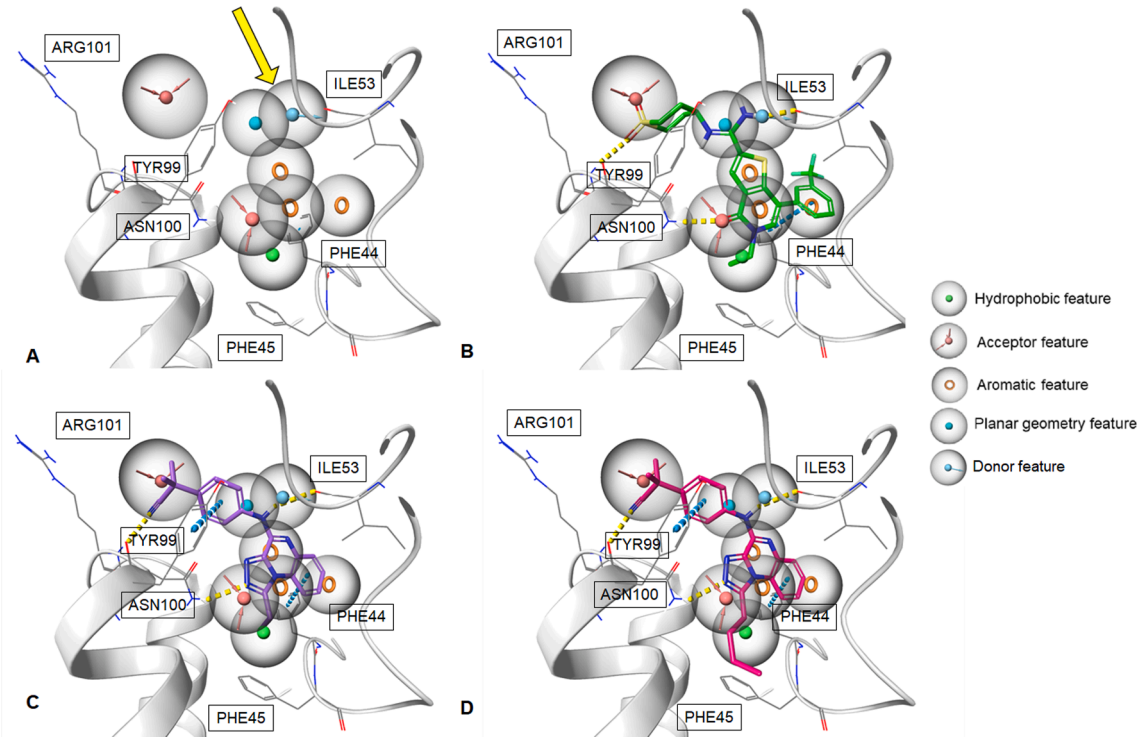

Fig. 10. Panel A) Representation of the optimized pharmacophore model with an additional donor feature i.e., "pharm-druglike2.1"; panel B) I-BRD9 superimposed on new "pharm-druglike2.1" model in the binding site of BRD9 (PDB code: 5F1H); panel C) **24** superimposed on the new "pharm-druglike2.1" model in the binding site of BRD9 (PDB code: 5F1H); panel D) **36** superimposed on the new "pharm-druglike2.1" model in the binding site of BRD9 (PDB code: 5F1H). H-bonds and π-π interactions are reported in yellow and cyan dotted lines, respectively. (For interpretation of the references to colour in this figure legend, the reader is referred to the web version of this article.)

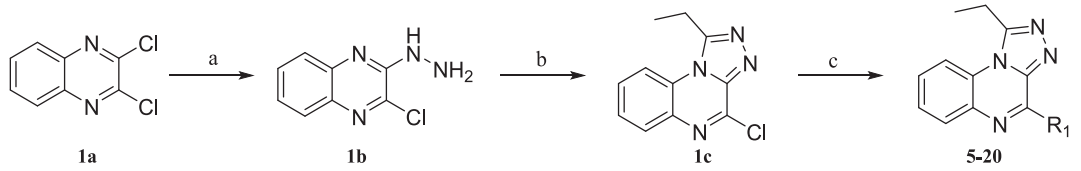

Scheme 1. Reagents and conditions: a) NH_2NH_2, EtOH, r.t., 20 h; b) $CH_3CH_2C(OC_2H_5)_3$, r.t., 16 h; c) $R_1B(OH)_2$, $(PPh_3)_2PdCl_2$, Cs_2CO_3, PCy_3, 1,4-dioxane/H_2O (8:2), 80 °C, overnight.

considering the "training set 2" (Figure S9) consisting of the same compounds reported in the "training set 1" with additional six representative triazoloquinoxaline-based compounds reported in this work. By applying the two obtained QSAR models to evaluate and predict the binding affinity of a "test set" (Figure S10), composed of BRD9 ligands for which the related experimental data are known, we detected an increased ability of the second model (R^2 = 0.86, Figure S11) in predicting the binding affinity of the test set compounds compared to the first model (R^2 = 0.66, Figure S11) (See Supporting Information for further details). These outcomes highlighted the robustness and reliability of the information achieved with the SAR study reported in this work.

2.5. Chemical synthesis

2.5.1. Synthesis of derivatives 5–20

The new set of 1-ethyl-[1,2,4]triazolo[4,3-*a*]quinoxaline derivatives was synthesized *via* an effective three steps synthetic route (reported in Scheme 1) that allowed rapid access to the desired compounds **5**–**20**. Specifically, the intermediate **1c**, synthesized as previously described by

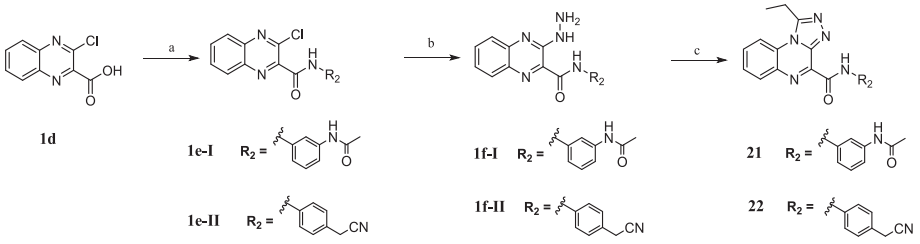

Scheme 2. Reagents and conditions: a) *N*-(3-aminophenyl)acetamide or 2-(4-aminophenyl)acetonitrile, EDC·HCl, HOBt, DMF, r.t., overnight; b) NH_2NH_2, EtOH, r.t., 20 h; c) $CH_3CH_2C(OC_2H_5)_3$, r.t., 16 h.

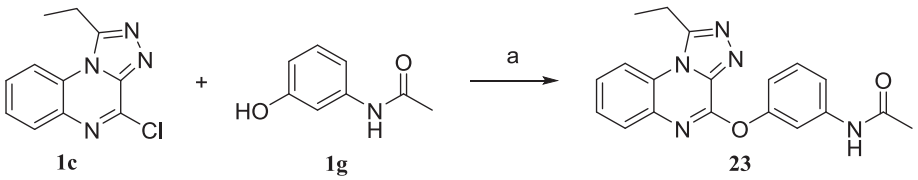

Scheme 3. Reagents and conditions: a) Cs_2CO_3, DMSO, 80 °C, 3 h.

us [15], was cross-coupled at 80 °C overnight with the selected organoboron species employing the Suzuki Miyaura reaction condition using bis(triphenylphosphine)palladium (II) dichloride as the catalyst, tricyclohexylphosphine as ligand, and cesium carbonate as the base. Following this procedure, the desired compounds **5**–**20** were obtained in variable yields (see Experimental section).

2.5.2. Synthesis of derivatives *21*–*23*

21 and **22** were obtained considering the commercial availability of the 3-chloroquinoxaline-2-carboxylic acid (**1d**). Thus, through a feasible synthetic procedure as shown in Scheme 2, compound **1d** was coupled to the chosen primary aromatic amine using standard peptide coupling conditions (EDC·HCl/HOBt). The obtained intermediate (**1e-I** or **1e-II**) was used for the following addition of hydrazine monohydrate at room temperature for 20 h to give **1f-I** or **1f-II** in good yields. The subsequent cyclization with triethyl orthopropionate overnight afforded the desired compounds **21** and **22** (see Experimental section).

In parallel, as previously described, to explore the ether linkage between the heterocyclic core and the aromatic ring at C-4, compound **23** was synthesized in high yields, as reported in Scheme 3, through nucleophilic substitutions on the intermediate **1c** (for the synthetic details see Experimental section).

2.5.3. Synthesis of derivatives *24*–*34*

For compounds **24**–**34**, featuring an amine linker, the synthetic route reported for the achievement of our first collection of triazoloquinoxaline derivatives was followed [15]. Specifically, for the synthesis of compound **27**, it was required a further synthetic step for the nitro group reduction employing Fe and NH_4Cl (Scheme 4).

2.5.4. Synthesis of derivatives *35*–*36*

Compounds **35** and **36** were synthesized as reported in Scheme 5. Specifically, in the second step, the construction of the three-fused scaffold was performed starting from the intermediate **1b** employing 1,1,1-triethoxybutane (for compound **1j**) or 1,1,1-triethoxypentane (for compound **1k**) depending on the length of the alkylic substituent in C-1. Finally, in the last step the S_NAr with the aromatic amine **1l** was carried out to obtain the desired compounds **35** and **36** (see Experimental section).

3. Conclusion

In this work, the application of a multidisciplinary workflow, guided by our developed 3D structure-based pharmacophore models, allowed us to identify a second generation of promising BRD9 binders and to trace an accurate structure–activity relationship (SAR). Hence, we optimized and updated the previously reported pharmacophore model (“pharm-druglike2”) by adding a hydrogen bond donor feature, which resulted indispensable for a selective BRD9 binding due to the interaction with the key Ile53 residue.

Specifically, we carefully explored the chemical space of the BRD9 binding pocket through the design and synthesis of a large collection of [1,2,4]triazolo[4,3-*a*]quinoxaline-based derivatives, analyzing the impact of different substitution patterns on the protein binding. Six new compounds (namely, **24**–**26**, **32**, **34** and **36**) emerged as new interesting BRD9 binders featuring IC_{50} values in the low micromolar range. Among these, **24** and its close derivative **36** showed an interesting selectivity profile on BRD9 over the high homologue BRD7. Biological investigations on a panel of human leukemia cell lines confirmed the potential therapeutic effect of **24** and **36**, with the best activity profile on CCRF-CEM cell line. Notably, **24** and **36** highlighted an evident modulation of BRPF1 (bromodomain and PHD finger containing 1), an important epigenetic target highly involved in carcinogenesis.

Summarizing, we believe that the new optimized 3D structure-based pharmacophore model, named “pharm-druglike2.1”, will aid the identification of novel promising BRD9 inhibitors with improved activity and, more importantly, with high selectivity over BRD7, which represents a crucial point in the discovery of BRD9 binders. The latter are urgently required both to get more insights into BRD9’s role in tumor environment and also for the design of new chemical degraders or SWI/SNF multi-target agents, aiming to overcome the issues related to the absence of potent phenotypical effects in cancer cell lines, also when using high affine/selective chemical probes. Finally, the here presented SAR study and the subsequent identification of novel dual BRD9/BRPF1 inhibitors, represent an excellent starting point for better understating the biological function of the targeted bromodomain proteins and for the development of new efficient and selective epidrugs.

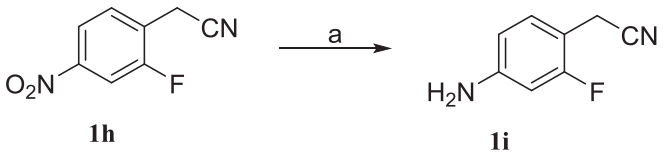

Scheme 4. Reagents and conditions: a) Fe, NH_4Cl, $EtOH/H_2O$, reflux, 2.5 h.

4. Experimental section

4.1. Computational studies

4.1.1. Library of screened compounds

Using CombiGlide software, a library of 589 1-ethyl-[1,2,4]triazolo[4,3-*a*]quinoxaline-based compounds was generated: 589 commercially available boronates were downloaded in .sdf format from Merck for the building of the library according to the synthetic route (Scheme 1). Subsequently, these compounds were prepared using LigPrep software (Schrödinger Suite) [28]. All the possible stereoisomers, tautomers, and protonation states at a pH = 7.4 ± 1.0 were generated for each compound, and the structures were minimized using OPLS 2005 force field. For all generated compounds, the related pharmacokinetic properties were calculated using the Qikprop program in the Schrödinger Suite [29]. After that, the new library was filtered using LigFilter, following the Lipinski filter to prioritize drug-like compounds and, finally, 376 compounds were selected to be subjected to subsequent molecular docking calculations. Compounds **21**–**36** were manually drawn by 2D Sketcher of Maestro (Schrödinger Suite) and then subjected to the same preparation steps applied for the above-mentioned library.

4.1.2. Virtual screening

Prior to perform docking calculations, the Protein Preparation Wizard workflow (Maestro, Schrödinger) was employed using the crystal structure of the BRD9 bromodomain in complex with BI-9564,

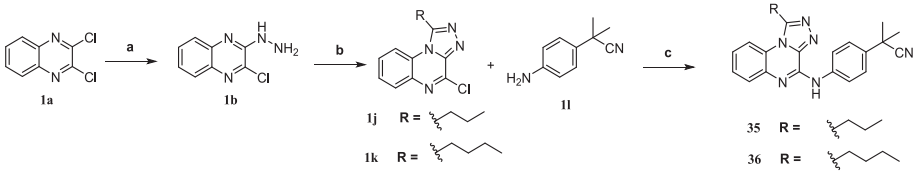

Scheme 5. Reagents and conditions: a) NH_2NH_2, EtOH, 25 °C, 20 h; b) 1,1,1-triethoxybutane (for **1j** and **35**) or 1,1,1-triethoxypentane (for **1k** and **36**), rt, 16 h; c) 110 °C MW, 6 min, DMSO.

the latter used as reference for grid box generation (PDB code:5F1H) [3]. All hydrogen atoms were added, and bond orders were assigned. Subsequently, the obtained library represented the input of molecular docking experiments, performed using the Virtual Screening Workflow tool in Schrödinger Suite and using Glide software[30–33] considering three level of precision: High-Throughput Virtual Screening scoring and sampling (HTVS), Standard Precision scoring and sampling phase (SP), Extra Precision scoring and sampling phase (XP). Specifically, the following scheme was applied for the three different levels:

- High-Throughput Virtual Screening scoring and sampling (HTVS), saved first 40% of compounds ranked by docking score;
- Standard Precision scoring and sampling phase (SP), saved first 40% of ranked compounds from HTVS;
- Extra Precision scoring and sampling phase (XP), generating 10 poses for each ligand and saved first 60% of ranked compounds from SP as final output.

Compounds **21**–**36** were submitted to molecular docking calculations employing the XP level and generating 10 poses for each compounds.

4.1.3. Pharmacophore screening

The output docking poses were subjected to a filtering round with the "pharm-druglike2" pharmacophore model, using Phase software [34]. In more detail, for each compound, the specific conformers arising from the molecular docking experiments were considered (namely skipping any further conformational search, and using the "score in place" option, in "Ligand and database screening" tool in Phase).

Finally, compounds **5**–**36** were selected by applying the following filters:

- Docking score < -4.2 kcal/mol (applying a cutoff of 4.0 kcal/mol, considering the best docking score value ~ -8.2 kcal/mol).
- PhaseScreen score > 1.25 (considering that PhaseScreen score value < 1 indicates no good match and PhaseScreen score value > 1.5 represents a good match).
- H-bond with Asn100.

4.1.4. Development of the new 3D structure-based pharmacophore model "pharm-druglike2.1"

Using the "Merged hypothesis" tool of Phase, all the features of the original "pharm-druglike2" were merged with a new donor feature identified by the applied tool considering the coordinates of nitrogen group of the amidine in I-BRD9 superimposed in the same coordinate system of the crystal structure of BRD9 (PDB code: 5F1H), to obtain "pharm-druglike2.1" [3].

4.2. Chemistry

4.2.1. Chemistry general information

All commercially available starting materials were used as purchased from Merck and Fluorochem without further purification. All solvents used for the synthesis were of HPLC grade (Merck). Chemical reactions were monitored on silica gel 60 F254 plates (Merck) and spots were visualized under UV light (λ = 254 nm). Proton (^{1}H) and carbon (^{13}C) NMR spectra were recorded on Bruker Avance 400, 500 or 600 MHz spectrometer at T = 298 K. All compounds were dissolved in 0.5 mL of $CDCl_3$, CD_3OD or DMSO-d_6 (Merck, 99.8 Atom % D). Chemical shifts (δ) are given in parts per million (ppm) relative to the solvent peak as internal reference: $CDCl_3$ (δH = 7.26 ppm/δC = 77.16 ppm), CD_3OD (δH = 3.31 ppm/δC = 49.00 ppm), or DMSO-d_6 (δH = 2.50 ppm/δC = 39.52 ppm). Coupling constants (*J*) are reported in Hertz (Hz). Signal patterns are reported as: s = singlet, d = doublet, t = triplet, q = quartet, p = quintet, h = sextet, m = multiplet, brs = broad, or a combination of the listed splitting patterns. High resolution mass spectrometry experiments were performed using a LTQ Orbitrap XL mass spectrometer (Thermo Scientific). Semi-preparative reversed-phase HPLC was performed on Agilent Technologies 1200 Series high-performance liquid chromatography using Luna C18 reversed-phase column (250 × 10 mm, 5 µm, 100 Å, flow rate = 4 mL/min, Phenomenex®). The binary solvent system (A/B) was as follows: 0.1% TFA in water (A) and 0.1% TFA in CH_3CN (B). The absorbance was detected at 240 nm. The purity of all biologically tested compounds (>96%) was determined following HPLC and NMR spectra evaluation. Microwave irradiation reactions were carried out in a dedicated CEM-Discover SP focused microwave synthesizer, operating with continuous irradiation power from 0 to 300 W utilizing the standard absorbance level of 300 W maximum power. Reactions were carried out in 10 mL sealed microwave glass vials. The Discover system also included controllable ramp time, hold time (reaction time), and uniform stirring. After the irradiation period, reaction vessels were cooled rapidly (60–120 s) to ambient temperature by air jet cooling.

*4.3. Syntheses of compounds **5**–**36***

*4.3.1. Synthesis of 2-chloro-3-hydrazinyl-quinoxaline (**1b**)*

To a solution of the commercially available 2,3-dichloroquinoxaline **1a** (1.0 equiv., 0.50 mmol) in ethanol (1.8 mL) was added hydrazine monohydrate (2.2 equiv., 1.10 mmol) and the reaction mixture was stirred overnight at room temperature. After completion, the mixture was precipitated in an ice bath and the resulting precipitate was collected, washed with ice-cold ethanol and dried to give **1b**, which was used without any further purification.

*4.3.2. General synthetic procedure (A) for the synthesis of the intermediate compounds **1c, 1j, 1k***

2-chloro-3-hydrazinyl-quinoxaline (**1b**) (1.0 equiv., 0.38 mmol) and the proper 1,1,1-triethoxyalkane derivative (i.e., 1,1,1-triethoxypropane, 1,1,1-triethoxybutane or 1,1,1-triethoxypentane) (10.0 equiv., 3.79 mmol) were stirred 16 h at room temperature. After completion, the resulting mixture was washed several times with cyclohexane and filtered. The precipitate was collected and dried under nitrogen atmosphere to give the desired intermediate compound, which was used without further purification.

*4.3.3. Synthesis of the intermediate 2-(4-amino-2-fluorophenyl)acetonitrile (**1i**)*

The commercially available 2-(2-fluoro-4-nitrophenyl)acetonitrile **1h** (1.0 equiv., 0.22 mmol), iron powder (3.0 equiv., 0.66 mmol), and NH_4Cl (5.0 equiv., 1.11 mmol) were dissolved in 1 mL of a solution of EtOH (40%) and H_2O (60%), and stirred at reflux for 2.5 h. After completion, the reaction mixture was filtered and DCM was added. The

organic phase was then washed with water and brine, dried over sodium sulfate, filtered, and finally condensed under reduced pressure to afford a residue which was used for the following step without further purification.

4.3.4. General synthetic procedure (B) for the synthesis of compounds 5–20

In a two-neck flask were added the intermediate 4-chloro-1-ethyl-[1,2,4]triazolo[4,3-*a*]quinoxaline (**1c**) (1.00 equiv., 0.25 mmol), the selected phenyl boronic acid (1.50 equiv., 0.38 mmol), PCy_3 (0.05 equiv. 0.01 mmol), $(PPh_3)_2PdCl_2$ (0.05 equiv. 0.01 mmol) and Cs_2CO_3 (3.90 equiv., 0.98 mmol). The flask was evacuated and backfilled with nitrogen three times. Then a degassed solution (2.2 mL) of 1,4-dioxane (80%) and water (20%) was added, and the mixture was stirred overnight at 80 °C under nitrogen atmosphere. After completion of the reaction, the mixture was cooled to room temperature, ethyl acetate was added and extracted with distilled water (x2) and brine (x1). The organic phase was dried over anhydrous Na_2SO_4, filtered and concentrated under vacuum. The crude was purified by semi-preparative reversed-phase HPLC by using the gradient conditions from 5% B to 100% B over 50 min, flow rate of 4 mL/min, λ = 240 nm, to achieve the final compounds **5**–**20**.

4.3.5. General synthetic procedure (C) for the synthesis of the intermediate compounds 1e-I and 1e-II

To a solution of the commercially available 3-chloroquinoxaline-2-carboxylic acid **1d** (1.1 equiv., 0.24 mmol) in dry DMF (1.9 mL), the proper amine (1.0 equiv., 0.23 mmol), EDC·HCl (2.8 equiv., 0.64 mmol), and HOBt (4.0 equiv., 0.91 mmol) were added. The reaction mixture was stirred at room temperature overnight under nitrogen atmosphere. After completion of the reaction, ethyl acetate was added and the organic phase was washed with a saturated solution of NH_4Cl (x3) and $NaHCO_3$ (x3). The organic layer was then dried over sodium sulfate, filtered, and condensed to afford a crude that was purified on silica gel column chromatography in hexane/ethyl acetate.

4.3.6. General synthetic procedure (D) for the syntheses of the intermediate compounds 1f-I and 1f-II

To a solution of the intermediate 3-chloro-*N*-substituted-quinoxaline-2-carboxamide compound (1.0 equiv., 0.05 mmol) in ethanol (0.7 mL), hydrazine monohydrate (2.2 equiv., 0.11 mmol) was added and the reaction mixture was stirred overnight at 25 °C. The crude was then precipitated in an ice bath. The resulting precipitate was filtered, washed with ice-cold ethanol and dried under nitrogen atmosphere to give the desired intermediate compound, which was then used without any further purification.

4.3.7. General synthetic procedure (E) for the synthesis of compounds 21 and 22

The intermediate compound 3-hydrazineyl-*N*-substituted-quinoxaline-2-carboxamide (1.0 equiv., 0.02 mmol) and triethyl orthopropionate (10.0 equiv., 0.22 mmol) were stirred overnight at room temperature. The resulting crude was then washed several times with cyclohexane and filtered. The precipitate was collected, dried and purified by semi-preparative reversed-phase HPLC by using the gradient conditions from 5% B to 100% B over 50 min, flow rate of 4 mL/min, λ = 240 nm, to achieve the final compounds **21** and **22**.

4.3.8. Synthesis of compound N-(3-((1-ethyl-[1,2,4]triazolo[4,3-a]quinoxalin-4-yl)oxy)phenyl)acetamide (23)

To a solution of 4-chloro-1-ethyl-[1,2,4]triazolo[4,3-*a*]quinoxaline (**1c**) (1.0 equiv., 0.18 mmol) in DMSO (0.5 mL) were added 3-acetamidophenol (1.0 equiv., 0.18 mmol) and cesium carbonate (1.2 equiv., 0.21 mmol). The reaction mixture was heated to 80 °C and stirred for 3 h. After cooling to room temperature, the mixture was diluted with dichloromethane (1.25 mL) and acidified with 1 N HCl. The obtained precipitate was filtered under reduced pressure and collected for further purification. In order to achieve the desired biology testing purity (>96%), semi-preparative reversed-phase HPLC was carried out by using the gradient conditions from 5% B to 100% B over 50 min, flow rate of 4 mL/min, λ = 240 nm.

4.3.9. General synthetic procedure (F) for the synthesis of compounds 24–36

A mixture of 4-chloro-1-alkyl-[1,2,4]triazolo[4,3-*a*]quinoxaline (**1c**, **1j** or **1k**) (1.0 equiv., 0.14 mmol) and the required aromatic amine (3.0 equiv., 0.41 mmol) in DMSO (0.4 mL) was heated under microwave irradiation at 110 °C for 6 min. After completion of the reaction, the mixture was diluted with DCM (1.0 mL) and acidified with 1 N HCl. The resulting precipitate was filtered under reduced pressure, the solid was collected and precipitated in methanol to give the desired compounds **24**–**36**. All the compounds were further purified by semi-preparative reversed-phase HPLC using the gradient conditions from 5% B to 100% B over 50 min, flow rate of 4 mL/min, λ = 240 nm.

4.4. BromoMELT™ assay

To analyze the selectivity of the most promising novel compound **24**, the BromoMELT™ assay was performed by Reaction Biology Corp. (PA, USA). This assay is a thermal melt stability assay for 76 bromodomain targets. A concentration of 10 μM of **24** was accounted for the assay. For further details, please visit https://www.reactionbiology.com/bromomelt-assay-kit. All raw data of the results are reported in Supplementary Information.

4.5. Binding assays on BRD9

AlphaScreen assays on BRD9 were carried out at Reaction Biology. Recombinant His-tagged bromodomain, test compounds, Histone H4 peptide (1–21) K5/8/12/16Ac-Biotin-OH for BRD9, was delivered to a 384-well OptiPlate and incubated at room temperature for 30 min with gentle shaking. Also, control compounds Bromosporine for BRD9 were employed and tested in 10-dose IC_{50} mode with 3-fold serial dilution starting at 10 uM. Streptavidine donor beads and nickel chelate acceptor beads were added to plates, followed by incubation in dark for 60 min with gentle shaking. Recombinant bromodomains, compounds, donor and acceptor beads were prepared as 4 × stock solution in the buffer of 50 mM HEPES-HCl, pH 7.5, 100 mM NaCl, 1 mg/ml BSA, 0.05% CHAPS and 0.5% DMSO. Alpha signal (Ex/ Em ¼ 680/520–620 nm) was measured with an Envision plate reader. Dose-response curve was fit with GraphPad Prism 9 using a nonlinear regression analysis model.

4.6. Binding assays on BRD7

The recombinant GST-tag BRD7 and Histone H3 (1–30) K4/18/23/27Ac-Biotin-OH were prepared in Hepes Buffer solution (BSP-31091), respectively at the final concentration of 2 ng/μL and 10 nM.

The tested or the reference compounds (each at a final concentration of DMSO%=0.5%) stimulated the mixture of the protein and the selected histone for 30 min at room temperature. After that, 10 μL of 250-fold diluted Glutathione AlphaLISA Acceptor Beads (PerkinElmer #AL109C) and 10 μL of 250- fold diluted Streptavidin Donor Bead (PerkinElmer #6760002) were added to plates (384-well Optiplates, Perkin Elmer) followed by incubation in the dark for 60 min with gentle shaking. In the end, Alpha signal (Ex/Em ¼ 680/520–620 nm) was measured with an Enspire microplate analyzer (Perkin Elmer).

4.7. Binding assays on BRPF1

The AlphaScreen assay was carried out using 2.5 μL of recombinant His-tagged bromodomain (627–746, final concentrations of 4 ng/μL), 20 nM H4(1–21)K5/8/12/16Ac-Biotin-OH peptide and 2.5 μL of test/reference compounds. The concentration of DMSO in each well was

maintained at a final concentration of 0.5%. The mixture was incubated for 30 min at room temperature. After the addition of the Nickel Chelate Acceptor Beads (125-fold dilution, PerkinElmer #AL108C) and Streptavidin Donor Bead (125-fold dilution, PerkinElmer #6760002) the plates were incubated in the dark for 60 min at room temperature and then were read on Enspire microplate analyzer (Perkin Elmer).

4.8. Biological evaluation

4.8.1. Cancer and healthy human cell cultures

Distinctive human leukemic cells were used as well-established preclinical *in vitro* models for this study. In particular, a panel of 5 leukemia cell lines (Kasumi-1, THP-1, CCRF-CEM, HL-60 and K-562 cells) representative of specific cellular models of leukemia was *ad hoc* selected. Kasumi-1 cells, herein used as model of Acute Myeloblastic Leukemia (AML), have been isolated from the peripheral blood of an acute myeloblastic leukemia Asian male patient. They were grown in RPMI-1640 (Gibco) supplemented with 20 % fetal bovine serum (FBS, Cambrex), L-glutamine (2 mM), penicillin (100 units/mL, Merck) and streptomycin (100 μg/mL). THP-1 cells, representing a model of Acute Monocytic Leukemia (AMoL) isolated from peripheral blood from an acute monocytic leukemia patient, were cultured in RPMI-1640 (Gibco) supplemented with 2-mercaptoethanol (0.05 mM, Merck), 10 % fetal bovine serum (FBS, Cambrex), L-glutamine (2 mM), penicillin (100 units/mL, Merck) and streptomycin (100 μg/mL). CCRF-CEM cells, a model of Acute Lymphoblastic Leukemia (ALL), are human T lymphoblasts isolated from the peripheral blood of a female, Caucasian 4-year-old with acute lymphoblastic leukemia (ALL). They were maintained in RPMI-1640 (Gibco) supplemented with 10 % fetal bovine serum (FBS, Cambrex), L-glutamine (2 mM), penicillin (100 units/mL, Merck) and streptomycin (100 μg/mL). HL-60 (promyeoloblasts isolated from the peripheral blood by leukopheresis from a 36-year-old, white, female with acute promyelocytic leukemia) herein used as a model of Acute Promyelocytic Leukemia (APL), and K-562 (lymphoblast cells isolated from the bone marrow of a 53-year-old chronic myelogenous leukemia patient) used as a model of Chronic Myelogenous Leukemia (CML), were cultured in Iscove's Modified Dulbecco's Medium (Gibco) supplemented with 20 % fetal bovine serum (FBS, Cambrex), L-glutamine (2 mM), penicillin (100 units/mL, Merck) and streptomycin (100 μg/mL). In the same experimental conditions, HaCaT and HDFa were used as human healthy control cultures. HaCaT, i.e., immortalized keratinocytes, were grown in DMEM (Invitrogen) supplemented with 10% fetal bovine serum (FBS, Cambrex), L-glutamine (2 mM), penicillin (100 units/mL, Merck) and streptomycin (100 μg/mL). Human Primary Adult Dermal Fibroblasts cells (HDFa) were directly obtained from the skin of a white male donator (PCS-201-012™) and purchased from ATCC (University Boulevard, Manassas, Virginia, USA). Cells were maintained in Fibroblast Basal Medium (ATCC) supplemented with Fibroblast Growth Kit–Low Serum (ATCC) containing recombinant human fibroblast growth factor (rh FGF, 5 ng/mL), L-glutamine (7.5 mM), ascorbic acid (50 μg/mL), hydrocortisone hemisuccinate (1 μg/mL), rh Insulin (5 μg/mL) and Fetal Bovine Serum (FBS, 2%). Moreover, Penicillin-Streptomycin-Amphotericin B Solution (Penicillin: 10 Units/mL, Streptomycin: 10 μg/mL, Amphotericin B: 25 ng/mL) was added. All the cell lines herein used for preclinical evaluations were kept at 37 °C in a humidified atmosphere containing 5% CO_2, according to ATCC manufactures.

4.8.2. Bioscreens in vitro and preclinical efficacy data

The activity of **24** and **36** compounds was investigated through the estimation of a "cell survival index", arising from the combination between cell viability and cell count [35]. Leukemia and healthy cells were inoculated in 96-microwell culture plates at a density of 10^4 cells/well and allowed to grow for 24 h. The medium was then replaced with fresh medium, and cells were treated for further 48 h with a range of concentrations (1 → 100 μM) of **24** and **36**. Following incubations, cell viability was evaluated using the MTT assay procedure, which measures the level of mitochondrial dehydrogenase activity using the yellow 3-(4,5-dimethyl-2-thiazolyl)-2,5-diphenyl-2*H*-tetrazolium bromide (MTT, Merck) as substrate. The assay is based on the redox ability of living mitochondria to convert dissolved MTT into insoluble purple formazan. Briefly, after the treatments, the medium was removed, and the cells were incubated with 20 μL/well of a MTT solution (5 mg/mL) for 1 h in a humidified 5% CO_2 incubator at 37 °C. The incubation was stopped by removing the MTT solution and by adding 100 μL/well of DMSO to solubilize the obtained formazan. Finally, the absorbance was monitored at 550 nm using a microplate reader (iMark microplate reader, Bio-Rad, Milan, Italy). Cell number was determined by TC20 automated cell counter (Bio-Rad, Milan, Italy), providing an accurate and reproducible total count of cells and a live/dead ratio in one step by a specific dye (trypan blue) exclusion assay. Bio-Rad's TC20 automated cell counter uses disposable slides, TC20 trypan blue dye (0.4% trypan blue dye w/v in 0.8% sodium chloride and 0.06% potassium phosphate dibasic solution) and a CCD camera to count cells based on the analyses of captured images. Once the loaded slide is inserted into the slide port, the TC20 automatically focuses on the cells, detects the presence of the trypan blue dye and provides the count. When cells are damaged or dead, trypan blue can enter the cell allowing living cells to be counted. Operationally, after treatments in 96-microwell culture plates, the medium was removed, and the cells were collected. 10 μL of cell suspension, mixed with 0.4% trypan blue solution at 1:1 ratio, were loaded into the chambers of disposable slides. The results are expressed in terms of total cell count (number of cells per mL). If trypan blue is detected, the instrument also accounts for the dilution and shows live cell count and percent viability. Total counts and live/dead ratio from random samples for each cell line were subjected to comparisons with manual hemocytometers in control experiments. The calculation of the concentration required to inhibit the net increase in the cell number and viability by 50% (IC_{50}) is based on plots of data ($n = 6$ for each experiment) and repeated five times (total $n = 30$).

5. Funding sources

The research leading to these results has received funding from AIRC under MFAG 2017 - ID. 20160 project – P.I. Lauro Gianluigi.

Declaration of Competing Interest

The authors declare that they have no known competing financial interests or personal relationships that could have appeared to influence the work reported in this paper.

Data availability

Data will be made available on request.

Appendix A. Supplementary data

Supplementary data to this article can be found online at https://doi.org/10.1016/j.bioorg.2023.106677.

References

[1] C.R. Clapier, B.R. Cairns, The biology of chromatin remodeling complexes, Annu. Rev. Biochem. 78 (2009) 273–304, https://doi.org/10.1146/annurev.biochem.77.062706.153223.

[2] C.-W. Chung, Small molecule bromodomain inhibitors: extending the druggable genome, Prog. Med. Chem. 51 (2012) 1–55, https://doi.org/10.1016/B978-0-12-396493-9.00001-7.

[3] L.J. Martin, M. Koegl, G. Bader, X.-L. Cockcroft, O. Fedorov, D. Fiegen, T. Gerstberger, M.H. Hofmann, A.F. Hohmann, D. Kessler, S. Knapp, P. Knesl, S. Kornigg, S. Müller, H. Nar, C. Rogers, K. Rumpel, O. Schaaf, S. Steurer, C. Tallant, C.R. Vakoc, M. Zeeb, A. Zoephel, M. Pearson, G. Boehmelt, D. McConnell, Structure-based design of an in vivo active selective BRD9 inhibitor,

J. Med. Chem. 59 (2016) 4462–4475, https://doi.org/10.1021/acs.jmedchem.5b01865.
[4] Y. Taniguchi, The bromodomain and extra-terminal domain (BET) family: functional anatomy of bet paralogous proteins, Int. J. Mol. Sci. 17 (2016) 1849, https://doi.org/10.3390/ijms17111849.
[5] M.A. Clegg, N.C.O. Tomkinson, R.K. Prinjha, P.G. Humphreys, Advancements in the development of non-BET bromodomain chemical probes, ChemMedChem 14 (2019) 362–385, https://doi.org/10.1002/cmdc.201800738.
[6] C. Kadoch, D.C. Hargreaves, C. Hodges, L. Elias, L. Ho, J. Ranish, G.R. Crabtree, Proteomic and bioinformatic analysis of mammalian SWI/SNF complexes identifies extensive roles in human malignancy, Nat. Genet. 45 (2013) 592–601, https://doi.org/10.1038/ng.2628.
[7] J.T. Lloyd, K.C. Glass, Biological function and histone recognition of family IV bromodomain-containing proteins, J. Cell. Physiol. 233 (2018) 1877–1886, https://doi.org/10.1002/jcp.26010.
[8] D.A. Levine, Integrated genomic characterization of endometrial carcinoma, Nature 497 (2013) 67–73, https://doi.org/10.1038/nature12113.
[9] C.G.A.R. Network, comprehensive genomic characterization of squamous cell lung cancers, Nature 489 (2012) 519–525, https://doi.org/10.1038/nature11404.
[10] A.F. Hohmann, L.J. Martin, J.L. Minder, J.-S. Roe, J. Shi, S. Steurer, G. Bader, D. McConnell, M. Pearson, T. Gerstberger, T. Gottschamel, D. Thompson, Y. Suzuki, M. Koegl, C.R. Vakoc, Sensitivity and engineered resistance of myeloid leukemia cells to BRD9 inhibition, Nat. Chem. Biol. 12 (2016) 672–679, https://doi.org/10.1038/nchembio.2115.
[11] E. Colarusso, E. Gazzillo, E. Boccia, A. Giordano, M.G. Chini, G. Bifulco, G. Lauro, 6-methylquinazolin-4(3H)-one based compounds as BRD9 epigenetic reader binders: a rational combination of in silico studies and chemical synthesis, Eur. J. Org. Chem. 2022 (2022) 251–260, https://doi.org/10.1002/ejoc.202200868.
[12] E. Colarusso, S. Ceccacci, M.C. Monti, E. Gazzillo, A. Giordano, M.G. Chini, M. G. Ferraro, M. Piccolo, D. Ruggiero, C. Irace, S. Terracciano, I. Bruno, G. Bifulco, G. Lauro, Identification of 2,4,5-trisubstituted-2,4-dihydro-3H-1,2,4-triazol-3-one-based small molecules as selective BRD9 binders, Eur. J. Med. Chem. 247 (2023), 115018, https://doi.org/10.1016/j.ejmech.2022.115018.
[13] S. De Vita, M.G. Chini, G. Bifulco, G. Lauro, Insights into the ligand binding to bromodomain-containing protein 9 (BRD9): a guide to the selection of potential binders by computational methods, Molecules 26 (2021) 7192, https://doi.org/10.3390/molecules26237192.
[14] M.G. Chini, G. Lauro, G. Bifulco, Addressing the target identification and accelerating the repositioning of anti-inflammatory/anti-cancer organic compounds by computational approaches, Eur. J. Org. Chem. 2021 (2021) 2966–2981, https://doi.org/10.1002/ejoc.202100245.
[15] M. Pierri, E. Gazzillo, M.G. Chini, M.G. Ferraro, M. Piccolo, F. Maione, C. Irace, G. Bifulco, I. Bruno, S. Terracciano, G. Lauro, Introducing structure-based three-dimensional pharmacophore models for accelerating the discovery of selective BRD9 binders, Bioorg. Chem. 118 (2022), 105480, https://doi.org/10.1016/j.bioorg.2021.105480.
[16] T.D. Crawford, V. Tsui, E.M. Flynn, S. Wang, A.M. Taylor, A. Côté, J.E. Audia, M. H. Beresini, D.J. Burdick, R. Cummings, L.A. Dakin, M. Duplessis, A.C. Good, M. C. Hewitt, H.-R. Huang, H. Jayaram, J.R. Kiefer, Y. Jiang, J. Murray, C. G. Nasveschuk, E. Pardo, F. Poy, F.A. Romero, Y. Tang, J. Wang, Z. Xu, L. E. Zawadzke, X. Zhu, B.K. Albrecht, S.R. Magnuson, S. Bellon, A.G. Cochran, Diving into the water: inducible binding conformations for BRD4, TAF1 (2), BRD9, and CECR2 bromodomains, J. Med. Chem. 59 (2016) 5391–5402, https://doi.org/10.1021/acs.jmedchem.6b00264.
[17] N.H. Theodoulou, P. Bamborough, A.J. Bannister, I. Becher, R.A. Bit, K.H. Che, C. W. Chung, A. Dittmann, G. Drewes, D.H. Drewry, L. Gordon, P. Grandi, M. Leveridge, M. Lindon, A.M. Michon, J. Molnar, S.C. Robson, N.C. Tomkinson, T. Kouzarides, R.K. Prinjha, P.G. Humphreys, Discovery of I-BRD9, a selective cell active chemical probe for bromodomain containing protein 9 inhibition, J. Med. Chem. 59 (2016) 1425–1439, https://doi.org/10.1021/acs.jmedchem.5b00256.
[18] P.G. Clark, L.C. Vieira, C. Tallant, O. Fedorov, D.C. Singleton, C.M. Rogers, O. P. Monteiro, J.M. Bennett, R. Baronio, S. Müller, D.L. Daniels, J. Méndez, S. Knapp, P.E. Brennan, D.J. Dixon, LP99: Discovery and synthesis of the first selective BRD7/9 bromodomain inhibitor, Angew. Chem. Int. Ed. 127 (2015) 6315–6319, https://doi.org/10.1002/ange.201501394.
[19] B. Altenburg, M. Frings, J.-H. Schöbel, J. Goßen, K. Pannen, K. Vanderliek, G. Rossetti, S. Koschmieder, N. Chatain, C. Bolm, Chiral analogues of PFI-1 as BET inhibitors and their functional role in myeloid malignancies, ACS Med. Chem. Lett. 11 (2020) 1928–1934, https://doi.org/10.1021/acsmedchemlett.9b00625.
[20] M. Ghiboub, A.M.I. Elfiky, M.P.J. de Winther, N.R. Harker, D.F. Tough, W.J. de Jonge, Selective targeting of epigenetic readers and histone deacetylases in autoimmune and inflammatory diseases: recent advances and future perspectives, J. Pers. Med. 11 (2021) 336, https://doi.org/10.3390/jpm11050336.
[21] M. Moustakim, P.G.K. Clark, D.A. Hay, D.J. Dixon, P.E. Brennan, Chemical probes and inhibitors of bromodomains outside the BET family, Medchemcomm 7 (2016) 2246–2264, https://doi.org/10.1039/c6md00373g.
[22] T. Brown, J. Swansbury, M.M. Taj, Prognosis of patients with t(8;16)(p11;p13) acute myeloid leukemia, Leuk. Lymphoma 53 (2012) 338–341, https://doi.org/10.3109/10428194.2011.614703.
[23] E.H. Demont, P. Bamborough, C.-W. Chung, P.D. Craggs, D. Fallon, L.J. Gordon, P. Grandi, C.I. Hobbs, J. Hussain, E.J. Jones, A. Le Gall, A.-M. Michon, D. J. Mitchell, R.K. Prinjha, A.D. Roberts, R.J. Sheppard, R.J. Watson, 1,3-dimethyl benzimidazolones are potent, selective inhibitors of the BRPF1 bromodomain, ACS Med. Chem. Lett. 5 (2014) 1190–1195, https://doi.org/10.1021/ml5002932.
[24] H. Shima, K. Yamagata, Y. Aikawa, M. Shino, H. Koseki, H. Shimada, I. Kitabayashi, Bromodomain-PHD finger protein 1 is critical for leukemogenesis associated with MOZ–TIF2 fusion, Int. J. Hematol. 99 (2014) 21–31, https://doi.org/10.1007/s12185-013-1466-x.
[25] K.F. Krämer, N. Moreno, M.C. Frühwald, K. Kerl, BRD9 inhibition, alone or in combination with cytostatic compounds as a therapeutic approach in rhabdoid tumors, Int. J. Mol. Sci. 18 (2017) 1537, https://doi.org/10.3390/ijms18071537.
[26] X. Yu, Z. Li, J. Shen, BRD7: a novel tumor suppressor gene in different cancers, Am. J. Transl. Res. 8 (2016) 742.
[27] S. Liu, B. Tong, J.W. Mason, J.M. Ostrem, A. Tutter, B.K. Hua, S.A. Tang, S. Bonazzi, K. Briner, F. Berst, F.J. Zécri, S.L. Schreiber, Rational screening for cooperativity in small-molecule inducers of protein–protein associations, bioRxiv (2023) 541439, https://doi.org/10.1101/2023.05.22.541439.
[28] LigPrep, Schrödinger LLC: New York, NY, USA, 2021.
[29] Qikprop, Schrödinger LLC: New York, NY, USA, 2021.
[30] R.A. Friesner, J.L. Banks, R.B. Murphy, T.A. Halgren, J.J. Klicic, D.T. Mainz, M. P. Repasky, E.H. Knoll, M. Shelley, J.K. Perry, Glide: a new approach for rapid, accurate docking and scoring. 1. Method and assessment of docking accuracy, J. Med. Chem. 47 (2004) 1739–1749, https://doi.org/10.1021/jm0306430.
[31] R.A. Friesner, R.B. Murphy, M.P. Repasky, L.L. Frye, J.R. Greenwood, T.A. Halgren, P.C. Sanschagrin, D.T. Mainz, Extra precision glide: Docking and scoring incorporating a model of hydrophobic enclosure for protein− ligand complexes, J. Med. Chem. 49 (2006) 6177–6196, https://doi.org/10.1021/jm051256o.
[32] T.A. Halgren, R.B. Murphy, R.A. Friesner, H.S. Beard, L.L. Frye, W.T. Pollard, J. L. Banks, Glide: a new approach for rapid, accurate docking and scoring. 2. Enrichment factors in database screening, J. Med. Chem. 47 (2004) 1750–1759, https://doi.org/10.1021/jm030644s.
[33] Glide, Schrödinger LLC: New York, NY, USA, 2021.
[34] Phase, Schrödinger LLC: New York, NY, USA, 2021.
[35] C. Irace, G. Misso, A. Capuozzo, M. Piccolo, C. Riccardi, A. Luchini, M. Caraglia, L. Paduano, D. Montesarchio, R. Santamaria, Antiproliferative effects of ruthenium-based nucleolipidic nanoaggregates in human models of breast cancer in vitro: insights into their mode of action, Sci. Rep. 7 (2017) 45236, https://doi.org/10.1038/srep45236.